Prediction of Liquid Circulation in Viscous Bubble Columns

A new theory to predict liquid circulation was derived and compared with applicable literature data. A single dimensionless group, $\bar{\epsilon}(gRd^2/\nu_c^2)$, is shown to control mixing intensity under low-viscosity conditions, but two separate groups ($\bar{\epsilon}$ and gRd^2/ν_c^2) are necessary for viscous systems. Closure was accomplished using the Prandtl model for Reynolds stress. Locally varying mixing length was taken to be proportional to bubble size and bubble concentration. The model was constructed based on the premise that two distinct zones exist: a mainly turbulent core joined to a thin viscous wall layer.

Richard G. Rice
Nicholas W. Geary
Department of Chemical Engineering
Louisiana State University
Baton Rouge, LA 70803

Introduction

Bubble columns are becoming widely used in biotechnology processes, such as fermentation, because of the favorable mass transfer properties and the low shear conditions imposed on the biological materials. Mass transfer and mixing properties are inextricably linked to the buoyancy-induced liquid circulation. It is not possible to predict the magnitude of liquid circulation with any degree of certainty, especially with highly viscous or non-Newtonian material (Kawase and Moo-Young, 1987; Ulbrecht et al., 1985). Moreover, the modeling of turbulent processes extant in all bubble columns has been somewhat empirical (Walter and Blanch, 1983; Walter, 1983; Ueyama and Miyauchi, 1979), without consideration of locally varying turbulence properties, such as Reynolds stresses.

More recently, Clark et al. (1987) and Anderson and Rice (1989) have effected closure by introducing Prandtl and von Karman turbulent stresses, respectively, to solve for local velocity profiles. In this paper, we extend the concepts introduced by these researchers and obtain the necessary conditions for circulation to occur. The velocity profile was expressed in terms of an elementary integral function. Under high-viscosity conditions, a simple asymptotic solution was obtained. The new theory was tested using the comprehensive measurements of Hills (1974), along with suitable high-viscosity data from other sources.

Theoretical Development

Figure 1 illustrates some of the physical conditions for this development. There are several approaches to modeling two-phase flow situations (Wallis, 1969) for tall columns, but the most general approach is the so-called "separated flow" model, which according to Ishii (1975), Ishii and Zuber (1979), and Rietema (1982), yield the following z-directed momentum balances on the continuous and discontinuous (gas) phases:

$$(1-\epsilon)\rho_c U_c \frac{\partial U_c}{\partial z} = -\nabla\cdot(1-\epsilon)T_c - (1-\epsilon)\nabla p - (1-\epsilon)\rho_c g + F_s \quad (1)$$

$$\epsilon\rho_d U_d \frac{\partial U_d}{\partial z} = -\nabla\cdot\ \epsilon T_c - \epsilon\nabla p - \epsilon\rho_d g - F_s \quad (2)$$

where F_s is the "slip force" or interfacial drag force per unit volume, and the local voidage is taken to depend only on radial position so that $\epsilon = f(r)$. Several power law models have been used to describe locally varying voidage, but the most popular to these (Ueyama and Miyauchi, 1979; Walter and Blanch, 1983; Yang et al., 1986) takes the form in terms of dimensionless radius ($\xi = r/R$):

$$\epsilon(\xi) = \bar{\epsilon}\left(\frac{m+2}{m}\right)(1-\xi^m) \quad (3)$$

Ueyama and Miyauchi (1979) suggest that m takes a value of around 2, but for bubbly flow conditions, the perforated-plate sparger data of Hills (1974) given in Figure 2 shows that values of m between 5 and 8 also give a good fit.

Our observations, and those of Ulbrecht and Baykara (1981), indicate the existence of a thin downflowing layer near (1-2 mm) the wall which is entirely bubble-free, mainly because of the restricted degrees of freedom for a bubble size of 2-4 mm to exist

Correspondence concerning this paper should be addressed to R. G. Rice.

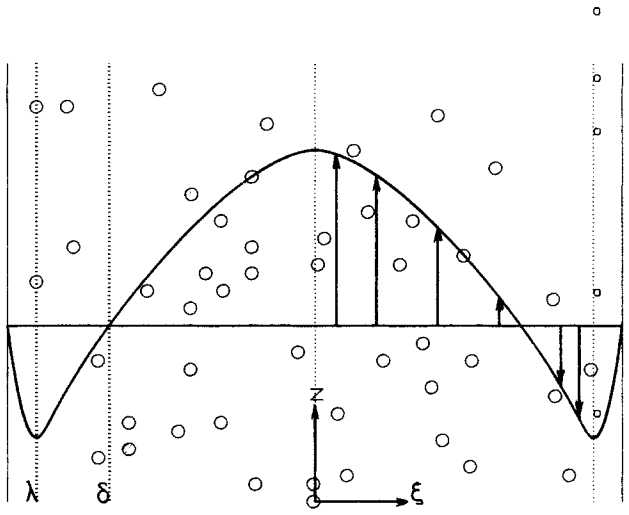

Figure 1. Typical viscous velocity profile, inversion position (δ), and maximum downflow velocity position (λ).

there. In dimensionless terms, the position of the maximum downflowing velocity is denoted by λ, and the inversion position (the demarcation between positive upflow and negative downflow velocity) is denoted as δ.

Thus, we propose two principal zones with voidage distributions as follows:

$$\epsilon(\xi) = \bar{\epsilon}\left(\frac{m+2}{m}\right)\frac{1}{\lambda^2}\left[1 - \left(\frac{\xi}{\lambda}\right)^m\right]; \quad \xi \le \lambda$$
$$\epsilon(\xi) = 0; \quad \xi \ge \lambda \tag{4}$$

If the phase densities are essentially constant, the lefthand sides of Eq. 1 and 2 are identically zero. Adding the two momentum equations, noting $\rho_d \ll \rho_c$, yields after integration in the region $0 \le \xi \le \lambda$:

$$T_c(\xi) = \frac{\rho_c g R}{2}[p' - 1]\xi + \frac{\rho_c g R}{\xi}\int_0^\xi \epsilon(x)\, x\, dx \tag{5}$$

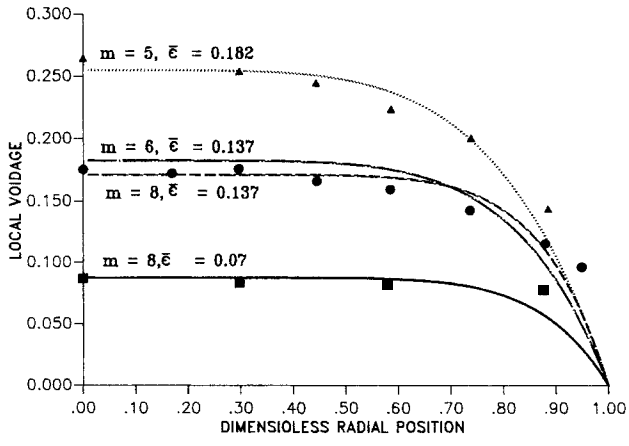

Figure 2. Local voidage profiles for Data of Hills (1974).

They correspond to superficial gas velocities of 19 (bottom curve), 38 (middle curve), and 64 (top curve) mm/s.

where we have defined the dimensionless axial pressure gradient to be

$$p' = \left(-\frac{dp}{dz}\right)/\rho_c g \tag{6}$$

Similarly, for the clear solution in the region $\lambda \le \xi \le 1$ (where an asterisk is used to denote this wall region):

$$T_c^*(\xi) = \frac{\rho_c g R}{2}[p' - 1]\xi + \frac{\rho_c g R}{\xi}\int_0^\lambda \epsilon(\xi)\xi\, d\xi \tag{7}$$

since for $\xi \ge \lambda$:

$$\int_0^\xi \epsilon(x)x\, dx = \int_0^\lambda \epsilon(x)x\, dx + \int_\lambda^\xi o \cdot x\, dx \tag{8}$$

It is clear from Eq. 8 that

$$\bar{\epsilon} = 2\int_0^\lambda \epsilon(\xi)\xi\, d\xi \tag{9}$$

Inserting the distributions from Equation (4) finally yields:

$$T_c(\xi) = \frac{\rho_c g R}{2}\left(\frac{2\bar{\epsilon}}{m\lambda^2}\right)\xi\left[1 - \left(\frac{\xi}{\lambda}\right)^m\right]; \quad \xi \le \lambda \tag{10}$$

$$T_c^*(\xi) = \frac{\rho_c g R}{2}\left(\frac{\bar{\epsilon}}{\lambda^2}\right)\left(\frac{\lambda^2 - \xi^2}{\xi}\right); \quad \xi \ge \lambda \tag{11}$$

These relations satisfy the required conditions for circulation, *viz.*, $T_c(0) = T_c(\lambda) = T_c^*(\lambda) = 0$.

Since λ defines the location of maximum downflow, we used the following zero stress requirement to eliminate p' following integration of Eq. 7:

$$T_c^*(\lambda) = \frac{\rho_c g R}{2}\left[(p' - 1)\lambda + \frac{\bar{\epsilon}}{\lambda}\right] = 0 \tag{12}$$

This can only be satisfied if:

$$\lambda = \sqrt{\bar{\epsilon}/(1 - p')} \tag{13}$$

In order for circulation to exist, the stress at the wall must exert a downward (anti-z) force so that

$$T_c^*(1) < 0 \tag{14}$$

This implies from Eqs. 11 and 13:

$$(p' - 1) + \bar{\epsilon} < 0 \tag{15}$$

hence, it is necessary that the dimensionless pressure gradient is always less than the mean hydrostatic head:

$$p' < (1 - \bar{\epsilon}) \tag{16}$$

for downflow at the wall to exist. This requirement also insures in Eq. 13 that $\lambda \le 1$.

Closure relations

To complete the integration for velocity profiles, we shall use the following strain models for the core and wall regions:

$$\frac{\mu_c}{R}\left(-\frac{\partial U_c}{\partial \xi}\right)+\rho_c\frac{l^2(\xi)}{R^2}\left(-\frac{\partial U_c}{\partial \xi}\right)^2=T_c(\xi);\quad \xi\le\lambda \tag{17}$$

$$\frac{\mu_c}{R}\left(-\frac{\partial U_c^*}{\partial \xi}\right)=T_c^*(\xi);\quad \xi\ge\lambda \tag{18}$$

Thus, viscous contributions are included in both, but only the core sustains locally varying turbulence of the Prandtl type.

The Prandtl model was originally based on the assumption that eddies move about in the fluid in a manner similar to molecules moving around in gases. This is a rather poor analogy for single-phase systems, but may be more appropriate in describing the movement of eddies generated by the chaotic movement of bubbles. The scale for such eddies are expected to lie in the range

$$l_d < l(\xi) < d_c \tag{19}$$

where the lower, or diffusive, limit is $l_d \sim (\nu_c^3/P_m)^{1/4}$, P_m being the energy dissipation per unit mass, which according to Baird and Rice (1975) is $P_m \sim U_{og}\cdot g$, hence $l_d \sim 0.1$ mm for water. The upper limit is taken to correspond to column diameter (d_c) which is the largest scale for an eddy to exist. Between these scales is the bubble diameter, which is small (3-5 mm) in the chain bubbling and bubbly flow regimes. As gas injection increases, however, the churn-turbulent condition arises, and this is followed by the slug flow regime. Transition to the latter two states depends on sparger type (especially number of holes, see Yoshitome and Shirai, 1970) and viscosity, but for water systems slugs begin appearing when superficial gas velocity exceeds 40 mm/s. Under such conditions, the bubble size can be of order column diameter so that eddy scale (in this model) becomes of this order.

We also expect that the number population density of bubbles should enhance eddy scaling, becoming larger as bubble concentration (hence number of interactions) increases. To account for these local variations, we propose, and later test, the following scaling relationship:

$$l(\xi) = d\cdot\epsilon(\xi)/\bar{\epsilon} \tag{20}$$

The conditions stated in Eq. 4 will automatically yield the common-sense result that $l = 0$ when $\xi \ge \lambda$, so that only viscous flow can exist in the narrow region near the wall. Moreover, scaling is such that the integral average of l is exactly equal to d, hence the necessity of placing $\bar{\epsilon}$ in the denominator.

Inserting the closure relations into Eq. 10 and 11 produces for $\xi \le \lambda$:

$$\frac{dU_c}{d\xi}=\frac{\nu_c R}{2l^2(\xi)}\left[1-\sqrt{1+\frac{2gRl^2(\xi)}{\nu_c^2}\cdot\beta(\xi)}\right] \tag{21}$$

where

$$\beta(\xi)=\frac{2\bar{\epsilon}}{m\lambda^2}\xi\left[=-\left(\frac{\xi}{\lambda}\right)^m\right] \tag{22}$$

and for $\xi \ge \lambda$:

$$\frac{dU_c^*}{d\xi}=\left(\frac{gR^2\bar{\epsilon}}{2\nu_c}\right)\left(\frac{\xi^2-\lambda^2}{\xi\lambda^2}\right) \tag{23}$$

The latter can be integrated directly using $U_c^*(1) = 0$, the nonslip condition at the wall:

$$U_c^*(\xi)=\left(\frac{gR^2\bar{\epsilon}}{4\nu_c\lambda^2}\right)(\xi^2-1-2\lambda^2\ln\xi);\quad \xi\ge\lambda \tag{24}$$

It is easy to show in the limit of Eq. 21 using L'Hôpital's rule that:

$$\lim_{\xi\to\lambda}\left(\frac{dU_c}{d\xi}\right)=0 \tag{25}$$

which is required for continuity.

It is theoretically possible to integrate the square root of the quartic relationship in Eq. 21 to yield elliptic integrals (Anderson and Rice, 1989), but the algebra is quite tedious. For the present, we shall integrate numerically using the final result in integral form:

$$U_c(\xi)-U_c^*(\lambda)=\int_\lambda^\xi\left(\frac{\nu_c R}{2}\right)\cdot\left(\frac{1-\sqrt{1+\dfrac{2gR}{\nu_c^2}l^2(x)\beta(x)}}{l^2(x)}\right)dx \tag{26}$$

where we use Eq. 24, since continuity requires that $U_c(\lambda) = U_c^*(\lambda)$, hence:

$$U_c^*(\lambda)=\left(\frac{gR^2\bar{\epsilon}}{4\nu_c\lambda^2}\right)(\lambda^2-1-2\lambda^2\ln\lambda) \tag{27}$$

Batch flow conservation

The requirement of mass conservation for a batch system is used to find λ for stipulated values of $\bar{\epsilon}$ and m as follows. The volumetric upflow rate must equal downflow so that the net liquid flow is nil, hence:

$$\int_0^\lambda(1-\epsilon)U_c\xi\,d\xi+\int_\lambda^1 U_c^*(\xi)\xi\,d\xi=0 \tag{28}$$

These can be put in more suitable form using integration by parts, and it is easy to show

$$0=-\frac{1}{16}\left(\frac{gR^2}{\nu_c}\right)\bar{\epsilon}\left(\frac{1+\lambda^4-2\lambda^2}{\lambda^2}\right)-\frac{1}{2}\int_0^\lambda\frac{dU_c}{d\xi}\xi^2\,d\xi+\frac{1}{2}\bar{\epsilon}\cdot\left(\frac{m+2}{m\lambda^2}\right)\int_0^\lambda\frac{dU_c}{d\xi}\xi^2\left[1-\frac{2}{m+2}\cdot\left(\frac{\xi}{\lambda}\right)^m\right]d\xi-\frac{1}{2}\bar{\epsilon}U_c^*(\lambda) \tag{29}$$

Inserting the gradient $dU_c/d\xi$ from Eq. 21 allows direct integration (numerical or analytical) of the batch flow condition. This yields an expression to find λ for given values of $\bar{\epsilon}$ and m.

Asymptotic solution for large viscosity

As molecular viscosity increases, the functional part of the argument within the square root of Eq. 21 becomes small, hence the square root can be given a series representation using the binomial expansion. Taking $f(\xi)$ to represent the functional part such that $f(\xi) < 1$:

$$\sqrt{1 + f(\xi)} = 1 + \frac{1}{2} f(\xi) - \frac{1}{8} f(\xi) + \cdots \tag{30}$$

This allows Eq. 21 to be written in a form suitable for term by term integration:

$$\frac{dU_c}{d\xi} = -\left(\frac{gR^2}{\nu_c}\right)\left(\frac{\bar{\epsilon}}{m\lambda^2}\right)\xi\left(1 - \left(\frac{\xi}{\lambda}\right)^m\right) + I^2(\xi)\left(\frac{g^2R^3}{\nu_c^3}\right)\left(\frac{\bar{\epsilon}}{m\lambda^2}\right)^2 \cdot \xi^2\left(1 - \left(\frac{\xi}{\lambda}\right)^m\right)^2 + \cdots \tag{31}$$

This form is quite useful for our purposes, since it clearly delineates the primary viscous contribution with the turbulent part as an added perturbation. Thus, the viscous part varies as $O(\bar{\epsilon})$, and the turbulent component varies as $O(\bar{\epsilon}^2)$. This sustains the correct behavior pattern as voidage increases, since it is known that chaotic behavior increases at large voidage.

The pivotal point for integration of the above is the continuity condition

$$U_c(\xi) = U_c^*(\lambda) \tag{32}$$

where $U_c^*(\lambda)$ is known exactly from Eq. 27. Applying this condition to evaluate the constant of integration and inserting $I(\xi)$ from Eq. 20 yield after integration:

$$\frac{U_c(\xi) - U_c(0)}{\left(\frac{gR^2\bar{\epsilon}}{\nu_c}\right)} \cong -\frac{\xi^2}{2m\lambda^2}\left(1 - \frac{2}{m+2}\frac{\xi^m}{\lambda^m}\right) + \bar{\epsilon}\left(\frac{gRd^2}{\nu_c^2}\right)\left(\frac{m+2}{m^2\lambda^4}\right)^2 \cdot \xi^3 \cdot F(\varphi) + \cdots \tag{33}$$

where

$$\varphi(\xi) = 1 - \left(\frac{\xi}{\lambda}\right)^m \tag{34}$$

$$F(\varphi) = \left[\varphi^4 + \frac{4m}{3m+3}\varphi^3 + \frac{4m \cdot 3m}{(3m+3)(2m+3)}\varphi^2 + \frac{8m^3(m+3\varphi)}{(3m+3)(2m+3)(m+3)}\right] \Big/ (4m+3) \tag{35}$$

$$\frac{U_c(0)}{\left(\frac{gR^2\bar{\epsilon}}{\nu_c}\right)} \cong \frac{1}{4}\left(\frac{2}{m+2} + \frac{\lambda^2 - 1 - 2\lambda^2 \ln \lambda}{\lambda^2}\right) - \bar{\epsilon}\left(\frac{gRd^2}{\nu_c^2}\right)\left(\frac{8}{\lambda^5}\right)\frac{(m+2)^2}{(4m+3)(3m+3)(2m+3)(m+3)} \tag{36}$$

where the last expression describes the central plume or centerline interstitial velocity of liquid.

Inserting the above into the batch flow condition, Eq. 29, leads to an implicit expression to compute λ:

$$0 = \frac{1}{8}\frac{\lambda^2}{m+4} - \frac{1}{16}\left(\frac{1 + \lambda^4 - 2\lambda^2}{\lambda^2}\right) + \bar{\epsilon}\left\{-\frac{1}{8}\left(\frac{\lambda^2 - 1 - 2\lambda^2 \ln \lambda}{\lambda^2}\right) - \frac{1}{8}\frac{\bar{\epsilon}}{(m+2)} - \left(\frac{gRd^2}{\nu_c^2}\right)\frac{(m+2)^2}{\lambda^3}\left(\frac{4!}{10}\right) \cdot \frac{1}{(4m+5)(3m+5)(2m+5)(m+5)}\right\} + \bar{\epsilon}^2\left\{\left(\frac{gRd^2}{\nu_c^2}\right)\frac{(m+2)^2}{\lambda^5}\left(\frac{4!}{2}\right) \cdot \frac{(m+3)}{(5m+5)(4m+5)(3m+5)(2m+5)(m+5)}\right\} \tag{37}$$

In the next section, we shall illustrate the behavior of the numerical integration of Eq. 21 coupled with Eq. 24, and compare it with experiments from the literature. The dimensionless group (gRd^2/ν_c^2) can be represented as the ratio of buoyancy and viscous force, hence it is an Archimedes number:

$$N_{Ar} = gRd^2/\nu_c^2 \tag{38}$$

Bubble size prediction

We next address the scale factor, d (bubble diameter). It is necessary to know bubble diameter to compare the present theory with literature data. Unfortunately, most researchers have not reported measured bubble sizes. For noncoalescing systems (e.g., water with trace surfactant) with low gas injection rates, the bubble diameter is essentially the size at formation. For small-hole perforated plates or punctured membranes (Flexispargers), Rice and Howell (1986) derived the following expression to compute bubble formation diameter, which accounts for viscous and surface tension effects

$$G^2\left[\frac{1}{2}(V^{1/3} - 1)\right] + N_\mu G\left[\frac{3}{2}(V^{2/3} - 1) - \ln V\right] = \frac{1}{2}(4\pi/3)^{1/3}\left[\frac{1}{2}(V^2 - 1) - 2(V - 1) + \ln V\right] \tag{39}$$

This function shows the bubble size is a monotonically increasing function of gas velocity, as illustrated in Figure 3. Here, V represents the ratio of final bubble volume (V_f) to nucleation bubble volume (V_o), where the nucleation bubble size is controlled solely by the balance between buoyancy and surface tension:

$$V = V_f/V_o = (d/d_o)^3 \tag{40}$$

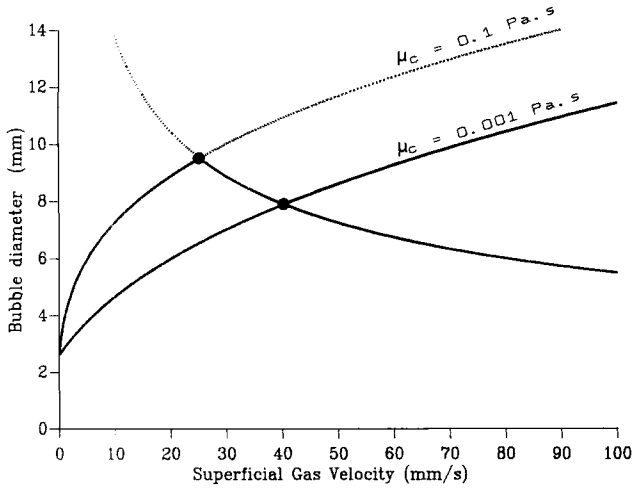

Figure 3. Predicted bubble size using formation dynamics intersecting breakage dynamics, Eqs. 39 and 44, based on Hills' column.

and the reference size d_o for an assumed spherical shape is:

$$d_o = (6d_H\sigma/\rho_c g)^{1/3} \tag{41}$$

where d_H is sparger hole diameter.

Gas flow rate enters via the dimensionless hole flow G, defined as

$$G = (AU_{og})/(jg^{1/2}V_o^{5/6}) \tag{42}$$

where j is the number of holes. Bubble frequency (s^{-1}) can be easily computed using $f = V_o^{1/6} \cdot V/G\sqrt{g}$).

The retarding effects of viscosity enters through the dimensionless group N_μ, defined as

$$N_\mu = 3\pi\left(\frac{4\pi}{3}\right)^{1/3}\frac{\nu_c}{(V_o g)^{1/2}} \tag{43}$$

The bubble size computed from the above relationship yields quite reasonable values for low gas velocities, as illustrated in Figure 3. However, as gas velocity increases, local turbulence stresses can overcome surface tension forces and bubble breakage occurs. Hinze (1955) developed a semiempirical relationship to forecast droplet (or bubble) size under turbulence conditions, and this was modified by Bhavaraju et al. (1978) to account for viscosity of the respective phases. More recently, this research group modified their work to account for phase density (Hesketh et al., 1987). The latter work predicts the Sauter mean diameter which can exist. Taking energy dissipation per unit mass as $P_m \sim U_{og} \cdot g$ (according to Baird and Rice, 1975), and ignoring gas-phase viscosity yields:

$$d \cong 0.43\left(\frac{\sigma^{0.6}}{[\rho_c^2\rho_d]^{0.2}}\right)\Big/(U_{og}g)^{0.4} \tag{44}$$

Thus, bubble size is expected to pass through a maximum as gas velocity increases, as illustrated for two distinct viscosities in Figure 3. A change of behavior occurs when the formation size (Eq. 39) intersects the turbulence size (Eq. 44) as denoted by the boldfaced point. We shall use the two relations to estimate bubble size in the manner implied by the curves in Figure 3. The transition zone (monotonically decreasing size) was measured by Yoshitome and Shirai (1970) to be in the range $10 < U_{og} < 50$ mm/s, which is close to the predictions shown in Figure 3. At higher gas velocities, large slugs form and bubble coalesence increases rapidly. The above bubble size relations cannot account for these effects. For large-diameter columns (>200 mm), slugging and churn turbulence occur at quite low gas velocities; so under these conditions, it may be appropriate to replace d with column diameter.

It is necessary to include an estimation of bubble size since this information is usually absent from the experimental data on liquid circulation, and this parameter is vital in the computation of Archimedes number.

Comparison with Experiment

We test the new theory in detail by comparing with the widely quoted data by Hills (1974). This two-phase literature offers quite rare qualities, in that it deals with not only local voidage profiles, but local liquid velocity as well (measured using the Pavlov-tube method). Also provided are such key data as gas flow rate, number and size of sparger holes, and average static voidage (manometric measurement). Its completeness perhaps explains why it has become the singularly most popular paper as a database for testing new theories. It is indeed remarkable that the bubble column literature is so replete with published work which contains missing, vital information. This of course makes testing of new theories quite difficult. Moreover, it is also clear that much otherwise useful data were taken from columns which were not perfectly aligned (e.g., Yang et al., 1986), as evidenced by the asymmetry of the profiles presented. Recently, Tinge and Drinkenburg (1986) and Rice and Littlefield (1987) have shown that minuscule levels of title (<0.5°) can cause enormous changes in flow patterns.

In preparation for comparison with experimental data, we rearrange the two forms of the theory to show that a single dimensionless group arises, *viz.*, $\bar{\epsilon}(gRd^2/\nu_c^2)$. To make the exact integral expression, Eq. 26, which is compatible with the asymptotic result in Eq. 33, we express both in terms of the dimensionless ratio $U_c(\xi)/U_c(0)$. Representing the integral in Eq. 26 as $I(x)$, the rearrangement to find $U_c(\xi)/U_c(0)$ is:

$$\frac{U_c(\xi)}{U_c(0)} = \left[1 + \int_\xi^\lambda I(x)\,dx/[-U_c^*(\lambda)]\right] \Big/ \left[1 + \int_0^\lambda I(x)\,dx/[-U_c^*(\lambda)]\right] \tag{45}$$

where we note that $U_c^*(\lambda) < 0$, i.e., downflowing liquid. Now, we introduce Eq. 27 for $U_c^*(\lambda)$, Eq. 20 for $I(\xi)$ and Eq. 4 for $\epsilon(\xi)$,

and rearrange to define the integral-function:

$$\frac{\int_{\xi}^{\lambda} I(x)\,dx}{[-U_c^*(\lambda)]} = \frac{\int_{\xi}^{\lambda}\left(\frac{1-\sqrt{1+4\bar{\epsilon}N_{Ar}\frac{(m+2)^2}{(m\lambda^2)^3}\cdot x\cdot\varphi(x)^3}}{\varphi(x)^3}\right)dx}{\frac{\bar{\epsilon}}{2}N_{Ar}\left(\frac{m+2}{m\lambda^3}\right)^2(1+2\lambda^2\ln\lambda-\lambda^2)} \quad (46)$$

where as before $\varphi(x) = 1 - (x/\lambda)^n$. The curve shown in Figure 1 was computed from Eq. 45 using $m = 8$, $\bar{\epsilon} = 0.01$, and $N_{Ar} = 10^4$.

Similarly, we rearrange the asymptotic result, Eq. 38, which also shows the appearance of the single dimensionless group

$$\bar{\epsilon}\left(\frac{gRd^2}{\nu_c^2}\right) = \bar{\epsilon}N_{Ar} \quad (47)$$

hence, we get

$$\frac{U_c(\xi)}{U_c(0)} \cong 1 + \frac{-\frac{\xi^2}{2m\lambda^2}\left(1-\frac{2}{m+2}\left(\frac{\xi}{\lambda}\right)^m\right)+\bar{\epsilon}N_{Ar}\left(\frac{m+2}{m^2\lambda^4}\right)^2\cdot\xi^3F(\varphi)}{\frac{1}{4}\left(\frac{2}{m+2}+\frac{\lambda^2-1-2\lambda^2\ln\lambda}{\lambda^2}\right)-\bar{\epsilon}N_{Ar}\left(\frac{8}{\lambda^5}\right)\frac{(m+2)^2}{(4m+3)(3m+3)(2m+3)(m+3)}} \quad (48)$$

where $F(\varphi)$ is defined by Eq. 35.

These results suggest comparing experimental data in terms of $\bar{\epsilon}N_{Ar}$ for measured or known values of m. As mentioned earlier, the data of Hills suggest that m is large (rather flat profile) in the bubbly regimes, and upon transition to churn turbulence, then m gradually takes values in the range 2-4. For small column diameters (<200 mm) in water systems, this transition to churn-slug conditions occurs when $U_{og} > 40$ mm/s. At the lower end, in the so-called chain bubbling region ($U_{og} < 4$ mm/s), circulation is expected to disappear. In this lower region, the voidage distribution becomes perfectly flat ($m \to \infty$), and the buoyancy driving force, which is the engine for circulation, disappears. The current model is applicable even under these circumstances. This is easy to see using Eqs. 36 and 53, which shows in the limit as $m \to \infty$, then $\lambda \to 1$ and $U_c(0) \to 0$.

At the upper end, in transition through churn turbulence to slug flow, the bubble size becomes in the limit equal to column diameter, so that the current model may still be applicable if d is replaced with column diameter, provided that one can carefully pinpoint transition values for $\bar{\epsilon}$, which are strongly tied to column diameter.

To explore the predictions from theory, we should investigate the following range from $\bar{\epsilon}N_{Ar}$:

$$1 < \bar{\epsilon}N_{Ar} < 10^6 \quad (49)$$

For the sake of completeness, we need to put the wall velocity, represented by Eq. 24, in proper dimensionless form, so we write

$$\frac{U_c^*(\xi)}{U_c(0)} = \frac{\left[\frac{\xi^2-1-2\lambda^2\ln\xi}{2\lambda^2\ln\lambda+1-\lambda^2}\right]}{1+\int_0^{\lambda} I(\xi)\,d\xi/[-U_c^*(\lambda)]} \quad (50)$$

where the integral in the denominator is computed according to Eq. 46 with the lower limit set at $\xi = 0$. Similarly, the wall velocity for the asymptotic solution, using Eq. 24 divided by the approximate centerline velocity (Eq. 36), yields:

$$\frac{U_c^*(\xi)}{U_c(0)} \cong 1 + \frac{\frac{1}{4}\left(\frac{\xi^2-1-2\lambda^2\ln\xi}{\lambda^2}\right)}{\left[\frac{1}{4}\left(\frac{2}{m+2}+\frac{\lambda^2\cdot 1-2\lambda^2\ln\lambda}{\lambda^2}\right)-\bar{\epsilon}N_{Ar}\left(\frac{8}{\lambda^5}\right)\frac{(m+2)^2}{(4m+3)(3m+3)(2m+3)(m+3)}\right]} \quad (51)$$

Limitations of theory

Inspection of Eqs. 45, 46 and 48 leads one to believe that $U_c(\xi)/U_c(0)$ depends only on a single dimensionless group, i.e., $\bar{\epsilon}N_{Ar} = \bar{\epsilon}(gRd^2/\nu_c^2)$. However, this is somewhat illusory, since λ also appears in these relations, and this quantity is computed from the batch flow condition. In the simplest case, Eq. 37 (which is the batch flow relationship for the asymptotic solution) shows the dependency of λ as:

$$\lambda = f(\bar{\epsilon}N_{Ar}, \bar{\epsilon}^2N_{Ar}, \bar{\epsilon}) \quad (52)$$

When $\bar{\epsilon} \ll 1$, and $N_{Ar} < 1$, the limiting value for λ can be estimated from Eq. 37:

$$\lambda \sim \sqrt{\frac{m+4}{m+2}}\left(1-\sqrt{\frac{2}{m+4}}\right)^{1/2} \quad (53)$$

Extending this, so that when $\bar{\epsilon} \ll 1$, and $N_{Ar} \gg 1$, then it is easy to see that:

$$\lambda \sim f(\bar{\epsilon}N_{Ar}) \quad (54)$$

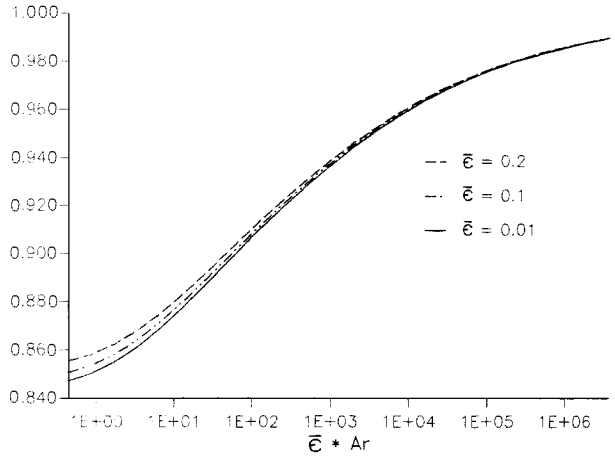

Figure 4. Maximum downflow position (λ) as a function of combined variable $\bar{\epsilon}\, N_{Ar}$.

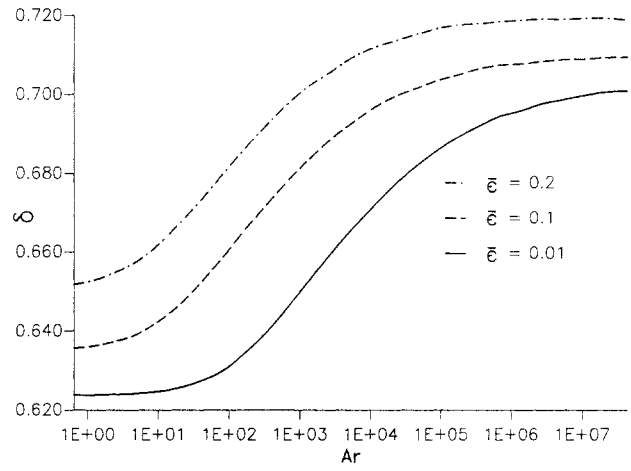

Figure 5. Inversion position (δ) as a function N_{Ar} for varying voidage ($\bar{\epsilon}$).

We illustrate these limitations in Figure 4 by showing λ vs. $\bar{\epsilon} N_{Ar}$ to pinpoint the range where only a single variable is necessary. Typical water columns sustain $N_{Ar} \sim 10^7$; so under such conditions, a single variable ($\bar{\epsilon} N_{Ar}$) is quite adequate for predicting performance. However, this is not the case for highly viscous systems. Hence, for viscous systems, λ depends on two separate variables $\bar{\epsilon}$ and N_{Ar}.

In Figure 5, we illustrate the behavior of inversion position δ, which was determined from Eq. 45 by requiring $U_c(\delta) = 0$. The present theory thus shows that essentially two asymptotes exist, depending on N_{Ar}. For highly viscous media ($N_{Ar} < 1$), then $\delta \sim 0.6$, while for large columns containing inviscid liquids, $\delta \sim 0.7$. These predictions are corroborated by the experimental observations of Ulbrecht et al. (1985) who suggested $\delta \sim 0.5$ and $\delta \sim 0.7$ for viscous and inviscid systems, respectively.

Data of J.H. Hills

Hills (1974) provides detailed measurements of voidage distribution and interstitial liquid velocity for three different sieve-type spargers. The most successful of these, called Plate B by Hills, contained 61 0.4-mm-dia. holes, with one central hole, the remainder being equally spaced around three concentric circles. The column was made of Perspex and had an internal diameter of 138 mm and a height of 1,370 mm. Local voidage and liquid velocity were measured at a position 600 mm above the sieve plate. Ordinary (Cambridge) tap water was used, and it was noted that the water was "hard" and needed no additional acidification for the conductivity-type voidage probe. Inspection of the voidage and velocity profile measurements indicate the existence of radial symmetry, hence the possibility of significant misalignment or tilt was absent.

For plate B, Hills reported five velocity profiles, along with the corresponding five data sets for voidage distributions using superficial gas velocities as follows: 19, 38, 64, 95 and 169 mm/s. The first two of these are clearly in the range of true bubbly flow, while the latter three are increasingly in the churn-turbulence regime. Hills noted that circulation existed for all of the five gas velocities noted above.

In Figure 2 we illustrate the fitting of the power law relationship in Eq. 3 to the low voidage data of Hills. It appears that m = 6-8 for bubbly flow. For the next highest velocity (64 mm/s), the voidage is fitted with $m \sim 5$ and becomes smaller still for higher gas velocity. We shall use these values as a basis for comparing predictions of liquid velocity. The mean voidage ($\bar{\epsilon}$) for each data set is indicated on the curves. In passing, we note that Wachi et al. (1987), Ueyama and Miyauchi (1979), and Yang et al. (1986) take $m \simeq 2$.

To compare our theoretical predictions with the velocity data of Hills, we shall need estimates of bubble size over the full gas velocity range noted above. Since there was no mention of bubble sizes observed, we shall use predictions based on Eqs. 39 and 44, which are presented in Figure 3 for the exact conditions of the experiments by Hills. Thus, in comparing velocity profiles (to follow), no adjustment of parameters was undertaken. The parameters m and $\bar{\epsilon}$ were determined from independent voidage experiments, and bubble size (d) was either calculated from theory or given as measured (e.g., Rietema and Ottengraf, 1970).

We compare our theory (Eq. 45) in dimensional form with the bubbly flow data from Hills in Figures 6 and 7. The comparisons are quite good, despite the fact that these low gas velocity data did not pass the consistency check applied by Hills (i.e., the

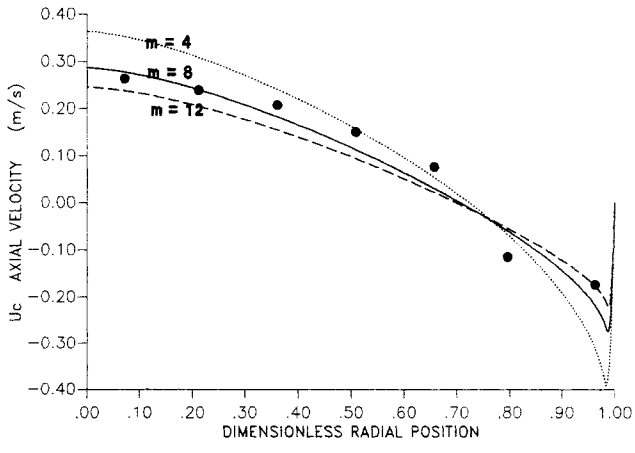

Figure 6. Measured velocity profile (Hills, 1974) vs. theory (Eqs. 45 and 50).

$m = 8 \pm 4$ at a superficial gas velocity of 19 mm/s, d = 5.8 mm.

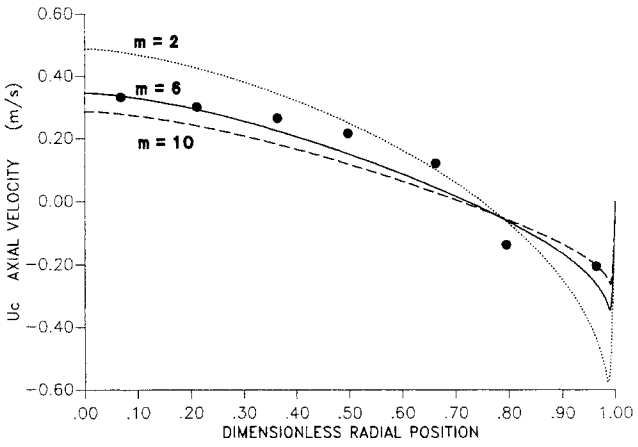

Figure 7. Measured velocity profile (Hills, 1974) vs. theory (Eqs. 45 and 50).
$m = 6 \pm 4$ at a superficial gas velocity of 38 mm/s, $d = 7.61$ mm.

batch flow condition). In these curves, we also illustrate the sensitivity to variations in the values of m.

For higher flows, the comparison is shown for a gas velocity 64 mm/s in Figure 8. This comparison is also quite good, indicating that the exponent for voidage distribution seems to be important in pinpointing flow regime.

It is not possible, in any straightforward way, to fit the newly proposed power law relation, Eq. 4, because of the presence of λ. However, since in the present situation, $\lambda \sim 1$, hence this factor will not significantly change the values of $\bar{\epsilon}$ and m required to match experimental voidage distribution. The structure imposed by Eq. 4 insures, however, that negative arguments can never appear under the square root in Eq. 21 and elsewhere.

High-viscosity experiments

There are several sources of high-viscosity data, but most of these data are not useful because of absent or unreported physical information. However, some of these experiments are quite complete, and one even includes bubble size (Rietema and Ottengraf, 1970). When bubble size was not provided, we used Eqs. 39 and 45 to estimate diameter.

In Figure 9, we show the high-viscosity velocity data reported by Rietema and Ottengraf (1970) and compared them to predictions from our theory (Eqs. 24 and 26, Eqs. 45, 46 and 50). The comparison in this case is excellent. We have taken the voidage exponent m to be 8, which was suggested by the low gas voidage data of Hills (1974). Additional details on this comparison are given in Table 1.

In Table 1, we also compare some illustrative centerline velocity measurements with the current theory, for viscosity ranging from 0.009 to 0.35 kg · m^{-1} · s^{-1}. The comparisons are quite satisfactory, indicating that the new theory seems to have a sound fundamental basis.

Comments and conclusions

Two-phase flow applications in chemical engineering are usually related to separation processes (flotation, fermentation, etc.) and, as such, the predictive models necessary are quite different in structure and scope from applications in other disciplines (e.g., high-speed gas-oil pipeline transmission, steam/water-phase changes in nuclear reactors, etc.). Thus, in separation technology, one must deal with high viscosity in tall bubble columns often operated in the batch mode. For continuous cocurrent or countercurrent separations, the injected superficial liquid velocities are usually quite low (<10 mm/s). In fact, it has been well documented (Baird and Rice, 1975) that axial dispersion (for small liquid injection rates) is unaffected by liquid injection, depending mainly on gas injection rates. This means of course that the batch mode can yield mixing information which is directly applicable to cocurrent or countercurrent bubble columns. This will not be the case for high-velocity (1,000 mm/s) liquid injection, such as used in the extensive work of Serizawa et al. (1975). In this work, the phenomena of "wall peaking" was observed, in what appeared to be a rather comprehensive experimental program. The measurement of wall-peaking or saddle-shaped voidage curves showed that the voidage maximum occurred very near the pipe wall, with a minimum voidage existing along the center line. It may well be the case that such behavior manifests itself as a true hydrody-

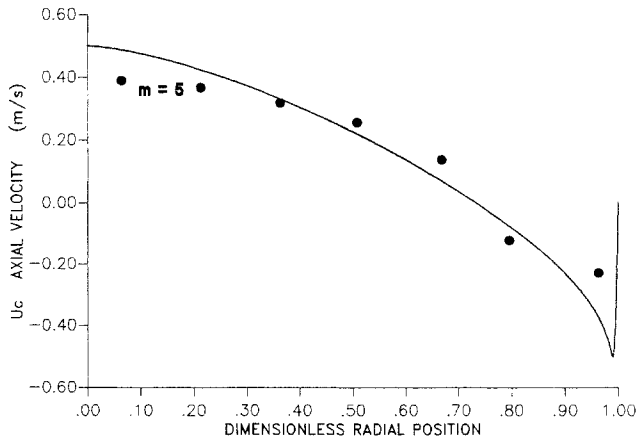

Figure 8. Measured velocity profile (Hills, 1974) vs. theory (Eqs. 45 and 50)
$m = 5$ at a superficial gas velocity of 64 mm/s, $d = 6.55$ mm.

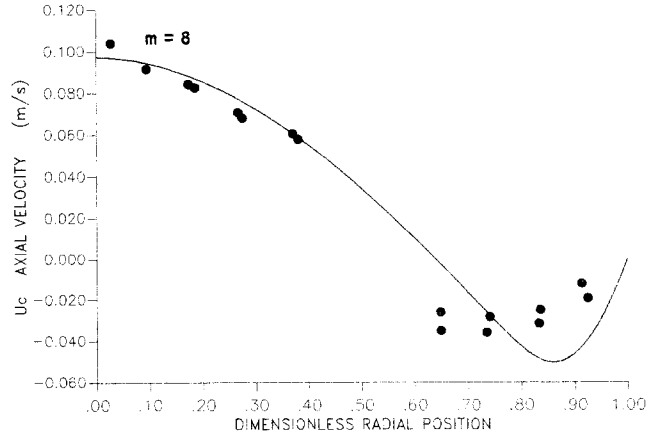

Figure 9. Measured velocity profile for high-viscosity (Rietema and Ottengraf, 1970; Table 1) vs. prediction from Eqs. 45 and 50.

Table 1. High-Viscosity, Centerline Liquid Velocity vs. Predictions from Theory ($m = 8$)

$\nu_c \cdot 10^{-4}$ (m^2/s)	$\bar{\epsilon}$	U_{og} (mm/s)	R (mm)	d (mm) Exp.	d (mm) Calc.	$U_c(0)$, m/s Exp.	$U_c(0)$, m/s Calc.	Comments
3.5	0.0118	0.3	110	5.4	—	0.10	0.0973	From Rietema and Ottengraf (1970): sparger with 19 injection needles; size unspecified
0.076	0.04	10	75	—	6.18	0.2	0.22	From Yoshitome and Shirai (1970): sparger with perforated plate with 37 0.8-mm-dia holes; a bubble size curve was presented, but not the corresponding viscosity; surface tension data provided
0.076	0.077	20	75	—	7.95	0.229	0.244	
0.076	0.156	50	75	—	7.86	0.38	0.36	

namic phenomenon, or it may be a consequence of some other physical quirk (misalignment, for example). Nonetheless, the approach taken here can still be applied if Eq. 4 is suitably replaced with saddle-shaped profiles.

The present work provides a new model to predict liquid circulation for bubbly and near bubbly conditions. It should be noted that the new theory was not fitted, since parameters were estimated from independent measurements and evolved naturally from the form given to the locally varying eddy size, $l(\xi)$. Additional tests on the new theory should be undertaken for high-viscosity systems, under conditions of perfect vertical alignment and using gas distributor devices of high efficiency.

Finally, we suspect that the exponent m may be continuously changing so that for ideal bubbly flow, $m \to \infty$, and for well-developed churn turbulence, $m \sim 2$, but for near bubbly flow, one should take $m \sim 8$. These observations suggest a structure like

$$m \simeq \kappa(\bar{\epsilon} N_{Ar})^{-1} + 2 \tag{55}$$

where $\kappa \sim 10^5$.

New theoretical and experimental work is necessary to predict voidage profiles from elementary first principles. The most fruitful avenue to do this is through the r-directed momentum relations.

Acknowledgment

This research was supported by the National Science Foundation (Grant #CBT-8820472), and their help is gratefully acknowledged.

Notation

A = column cross-sectional area, m^2
d = bubble diameter, m
d_c = column diameter, m
F_s = slip force, N/m^3
f = bubble frequency, s^{-1}
g = acceleration due to gravity, m/s^2
G = dimensionless gas rate from distributor hole
j = number of holes in distributor
m = exponent, Eqs. 3 and 4
N_{Ar}, Ar = Archimedes number (gRd^2/ν_c^2)
p_m = rate of energy dissipation per unit mass, m^2/s^3
p = pressure, kPa
p' = dimensionless pressure gradient, Eq. 6
r = radial coordinate, m
R = column radius, m
T_c = continuous-phase stress tensor, kPa
U_c = continuous-phase interstitial velocity, m/s
U_d = dispersed-phase interstitial velocity, m/s
U_{og} = superficial gas velocity, m/s
V = bubble volume ratio, V_f/V_o
V_f = final bubble volume, m^3
V_o = nucleation bubble volume, m^3

Greek letters

β = function defined by Eq. 22
δ = inversion position, dimensionless
ϵ = gas voidage
$\bar{\epsilon}$ = mean gas voidage
λ = position of wall velocity maximum, dimensionless
μ_c = continuous-phase molecular viscosity, kg/m · s
ν_c = continuous-phase kinematic viscosity, m^2/s
ξ = dimensionless radial coordinate, r/R
ρ_c, ρ_d = continuous- and dispersed-phase densities, kg/m^3
σ = interfacial surface tension, N/m

Superscript

* = associated with annular downflowing region

Literature Cited

Anderson, K. G., and R. G. Rice, "Local Turbulence Model for Predicting Circulation Rates in Bubble Columns," *AIChE J.*, **35,** 514 (1989).
Baird, M. H. I., and R. G. Rice, "Axial Dispersion in Large Unbaffled Columns," *Chem. Eng. J.*, **9,** 171 (1975).
Bhavaraju, S. M., T. W. F. Russell, and H. W. Blanch, "The Design of Gas Sparged Devices for Viscous Liquid Systems," *AIChE J.*, **24,** 454 (1978).
Clark, N. N., C. M. Atkinson, and R. L. C. Flemmer, "Turbulent Circulation in Bubble Columns," *AIChE J.*, **33,** 515 (1987).
Hesketh, R. P., T. W. F. Russell, and A. W. Etchells, "Bubble Size in Horizontal Pipelines," *AIChE J.*, **33,** 663 (1987).
Hills, J. H., "Radial Nonuniformity of Velocity and Voidage in a Bubble Column," *Trans. I. Chem. Eng.*, **52,** 1 (1974).
Hinze, J. O., "Fundamentals of the Hydrodynamic Mechanism of Splitting in Dispersion Processes," *AIChE J.*, **1,** 189 (1955).
Ishii, M., *Thermo-Fluid Dynamic Theory of Two-Phase Flow*, Eyrolles, Paris (1975).
Ishii, M., and N. Zuber, "Drag Coefficient and Relative Velocity in Bubbly, Droplet or Particulate Flows," *AIChE J.*, **25,** 834 (1979).
Kawase, Y., and M. Moo-Young, "Theoretical Prediction of Gas Hold-Up in Bubble Columns with Newtonian and Non-Newtonian Fluids," *Ind. Eng. Chem. Res.*, **26,** 933 (1987).
Rice, R. G., and S. W. Howell, "Bubble Formation from Elastic Holes," *Chem. Eng. Comm.*, **59,** 229 (1987).
Rice, R. G., and M. A. Littlefield, "Dispersion Coefficients for Ideal Bubbly Flow in Truly Vertical Bubble Columns," *Chem. Eng. Sci.*, **42,** 2045 (1987).
Rietema, K., "Science and Technology of Dispersed Two-Phase Systems: I. and II," *Chem. Eng. Sci.*, **37,** 1125 (1982).
Rietema, K., and S. P. P. Ottengraf, "Laminar Liquid Circulation and Bubble Street Formation in a Gas-Liquid System," *Trans. Instn. Chem. Engrs.*, **48,** T54 (1970).
Serizawa, A., I. Kataoka, and I. Michiyoshi, "Turbulence Structure of Air-Water Bubbly Flow - I. Measuring Techniques," *Int. J. Multiphase Flow*, **2,** 221 (1975).
Ibid, "II. Local Properties," **2,** 235 (1975).
Ibid, "III. Transport Properties," **2,** 247 (1975).

Tinge, J. T., and A. A. H. Drinkenburg, "The Influence of Slight Departures from Vertical Alignment on Liquid Dispersion and Gas Hold-Up in a Bubble Column," *Chem. Eng. Sci.*, **41,** 165 (1986).
Ueyama, K., and T. Miyauchi, "Properties of Recirculating Turbulent Two Phase Flow in Gas Bubble Columns," *AIChE J.*, **25,** 258 (1979).
Ulbrecht, J. J., and Z. S. Baykara, "Significance of the Central Plume Velocity for the Correlation of Liquid Phase Mixing in Bubble Columns," *Chem. Eng. Comm.*, **10,** 165 (1981).
Ulbrecht, J. J., Y. Kawase, and K. F. Auyeung, "More on Mixing of Viscous Liquids in Bubble Columns," *Chem. Eng. Comm.*, **35,** 175 (1985).
Wachi, S., H. Morikawa, and K. Ueyama, "Gas Holdup and Axial Dispersion in Gas-Liquid Concurrent Bubble Column," *J. Chem. Eng. Japan*, **20,** 309 (1987).
Wallis, G. B., *One-Dimensional Two-Phase Flow*, McGraw-Hill, New York (1969).
Walter, J. F., "Bubble Break-Up and Mass Transfer in Gas-Liquid Contactors," PhD Thesis, Univ. of California, Berkeley (1983).
Walter, J. F., and H. W. Blanch, "Liquid Circulation Patterns and Their Effect on Gas Hold-Up and Axial Mixing in Bubble Columns," *Chem. Eng. Comm.*, **19,** 243 (1983).
Yang, Z., U. Rustemeyer, R. Buchholz, and U. Onken, "Profile of Liquid Flow in Bubble Columns," *Chem. Eng. Comm.*, **49,** 51 (1986).
Yoshitome, H., and T. Shirai, "The Intensity of Bulk Flow in a Bubble Bed," *J. Chem. Eng. Japan*, **3,** 29 (1970).

Manuscript received Apr. 2, 1990, and revision received June 26, 1990.